

THE EXTREME SMALL SCALES: DO SATELLITE GALAXIES TRACE DARK MATTER?

DOUGLAS F. WATSON¹, ANDREAS A. BERLIND^{1,2}, CAMERON K. MCBRIDE¹, DAVID W. HOGG^{3,4}, TAO JIANG³

Draft version February 7, 2012

ABSTRACT

We investigate the radial distribution of galaxies within their host dark matter halos as measured in the Sloan Digital Sky Survey by modeling their small-scale clustering. Specifically, we model the Jiang et al. (2011) measurements of the galaxy two-point correlation function down to very small projected separations ($10 \leq r \leq 400h^{-1}\text{kpc}$), in a wide range of luminosity threshold samples (absolute r -band magnitudes of -18 up to -23). We use a halo occupation distribution (HOD) framework with free parameters that specify both the number and spatial distribution of galaxies within their host dark matter halos. We assume one galaxy resides in the halo center and additional galaxies are considered satellites that follow a radial density profile similar to the dark matter Navarro-Frenk-White (NFW) profile, except that the concentration and inner slope are allowed to vary. We find that in low luminosity samples ($M_r < -19.5$ and lower), satellite galaxies have radial profiles that are consistent with NFW. $M_r < -20$ and brighter satellite galaxies have radial profiles with significantly steeper inner slopes than NFW (we find inner logarithmic slopes ranging from -1.6 to -2.1 , as opposed to -1 for NFW). We define a useful metric of concentration, $M_{1/10}$, which is the fraction of satellite galaxies (or mass) that are enclosed within one tenth of the virial radius of a halo. We find that $M_{1/10}$ for low luminosity satellite galaxies agrees with NFW, whereas for luminous galaxies it is $2.5 - 4$ times higher, demonstrating that these galaxies are substantially more centrally concentrated within their dark matter halos than the dark matter itself. Our results therefore suggest that the processes that govern the spatial distribution of galaxies, once they have merged into larger halos, must be luminosity dependent, such that luminous galaxies become poor tracers of the underlying dark matter.

Subject headings: cosmology: theory — galaxies: fundamental parameters — large-scale structure of universe — methods: statistical — surveys

1. INTRODUCTION

Determining the relationship between the spatial distributions of galaxies and dark matter remains one of the central problems of theoretical and observational cosmology. The radial distribution of galaxies within their host dark matter halos dictates the correlation function on scales smaller than the virial radii of the largest dark matter halos ($\lesssim 1h^{-1}\text{Mpc}$). Therefore, the measured galaxy correlation function itself is a powerful tool for shedding light on how galaxies trace the underlying dark matter within halos.

The halo occupation distribution (HOD) framework has been established as a robust method for modeling galaxy clustering by simply characterizing the biased relationship between galaxies and mass (see, e.g., Peacock & Smith 2000; Scoccimarro et al. 2001; Berlind & Weinberg 2002; Cooray & Sheth 2002; Zheng et al. 2005). The HOD describes this relation by specifying the probability distribution $P(N|M)$ that a halo of mass M contains N galaxies, along with a prescription for the spatial distribution of galaxies within halos. For this latter component, it is typically assumed that a single ‘central’ galaxy lives at the center of each halo, with additional ‘satellite’ galaxies tracing the dominant dark matter component. This assumption

has been used successfully to model galaxy clustering on scales larger than $r \sim 100h^{-1}\text{kpc}$ (e.g., Zehavi et al. 2004, 2005b, 2011; Zheng et al. 2007, 2009). However, Watson et al. (2010) showed that this assumption does not work to explain the smaller-scale clustering of luminous red galaxies (LRGs) in the Sloan Digital Sky Survey (SDSS; York et al. 2000). In order to achieve a good fit to the clustering of LRGs on scales smaller than $\sim 100h^{-1}\text{kpc}$ (measured by Masjedi et al. 2006), they found that the radial profile of satellite LRGs must have a much steeper inner slope compared to the Navarro-Frenk-White (NFW; Navarro et al. 1997) dark matter profile. Watson et al. (2010) concluded that the distribution of satellite LRGs within halos is better described by an isothermal distribution.

Recently, Jiang et al. (2011) measured the projected two-point correlation function $w_p(r_p)$ for several luminosity samples from the SDSS, extending the measurements done by Zehavi et al. (2011) on intermediate scales ($\sim 0.1 - 40h^{-1}\text{Mpc}$) down to extremely small galaxy-galaxy separations ($0.01 - 7h^{-1}\text{Mpc}$). Our motivation for this paper is to model the innermost data points ($0.01 - 0.4h^{-1}\text{Mpc}$) in the same vein as Watson et al. (2010, hereafter W10) to see if there is a luminosity dependence of the radial profile of satellite galaxies.

The paper is laid out as follows. In §2, we review the Jiang et al. (2011, hereafter J11) measurements. In §3, we discuss our modeling method in the following manner: in §3.1 we provide an overview of the general technique used to model the small-scale correlation function; in §3.2 we revisit the W10 four-parameter PNM model that allows the the probability distribution $P(N|M)$ to vary,

¹ Department of Physics and Astronomy, Vanderbilt University, 1807 Station B, Nashville, TN 37235

² Alfred P. Sloan Fellow

³ Center for Cosmology and Particle Physics, Department of Physics, New York University, New York, NY, 10003

⁴ Max-Planck-Institut für Astronomie, Königstuhl 17, D-69117 Heidelberg, Germany

and the five-parameter PNMCG model that also allows the radial distribution of galaxies within halos to vary. We present our results in §4. Finally, we summarize and discuss the implications of our results in §5. Throughout the paper, we assume a Λ CDM cosmology with $\Omega_m = 0.25$, $\Omega_\Lambda = 0.75$, $\Omega_b = 0.04$, $h_0 = 0.7$, $\sigma_8 = 0.8$, $n_s = 1.0$.

2. DATA

J11 measured the projected two-point correlation function down to very small scales ($0.01 < r < 7h^{-1}\text{Mpc}$) for a large range of volume-limited galaxy luminosity threshold samples. Galaxy number densities and median redshifts for each sample can be found in Table 1. These samples are constructed from the NYU VAGC (Blanton et al. 2005) V7.2 data (Abazajian et al. 2009) which contains 8.6×10^5 SDSS Main Sample galaxies (Strauss et al. 2002). Spectra for each luminosity threshold sample are cross-correlated with the full imaging sample to compute $w_p(r_p)$ (details of the method can be seen below). The full imaging sample consists of $\sim 10^8$ galaxies drawn from the SDSS imaging catalog.

Measuring $w_p(r_p)$ on very small scales is a non-trivial task. The SDSS spectroscopic sample suffers from incompleteness due to the physical size of the fiber-optic cables, which impede the ability to take spectra of two galaxies closer than $55''$ on the sky. These “fiber collisions” thus result in a minimum pair separation of $55''$. This effect is partially mitigated by the tiling method (Blanton et al. 2003), which overlaps spectroscopic plates in order to yield full sky coverage. In plate overlap regions, galaxy pairs closer than $55''$ can be recovered. However, this still leaves $\sim 9\%$ of galaxies without measured redshifts (J11) and this can strongly affect clustering measurements on very small scales. Following the approach described in Masjedi et al. (2006, 2008), J11 used a cross-correlation technique between the imaging and spectroscopic samples to correct for fiber collisions and obtain unbiased $w_p(r_p)$ measurements down to the $10h^{-1}\text{kpc}$ scale. Details of the method can be found in §3 of J11.

A second potential problem that affects very small scales is that galaxies may be overlapping and the light within this region needs to be properly distributed between the two galaxies. This is known as “deblending”. M06 found a systematic error in the SDSS pipeline wherein too much light was allocated to the dimmer of the two galaxies. As a result, a galaxy that may have been too dim to make the LRG brightness cut could now be included in the sample. This increased the number of small-scale pairs and boosted the correlation function on very small scales. M06 quantified this effect and corrected their measurements accordingly. Since the physical sizes of galaxies decrease rapidly with decreasing luminosity, this photometric deblending error diminishes in lower luminosity samples. For this reason, J11 ignored this effect in the luminosity samples they considered ($M_r < -18$ through -21). Nevertheless, we estimate the maximum effect of deblending by applying the M06 LRG correction to the $M_r < -21$ sample and repeating our analysis. We find that our results do not change qualitatively.

We restrict ourselves to modeling the J11 data points from $\sim 10 - 400h^{-1}\text{kpc}$. These can be seen in Figure 1, which shows $w_p(r_p)$ scaled by an r_p^{-1} power law, with each panel corresponding to a distinct luminosity

threshold. The bottom right panel of Figure 1 shows the LRG data points measured by M06 and modeled by W10. Along with these 9 data points used in our modeling, we also incorporate the measured number density for each luminosity sample (see Table 1), providing a tenth data point. We use the full covariance matrices from the 9 J11 $w_p(r_p)$ data points for each sample, which were estimated using jackknife resampling of 50 regions on the sky. The same jackknife samples were used to estimate the error on each calculated number density.

3. REVIEW OF THE METHOD

3.1. The HOD and the Galaxy 2PCF

Here we briefly review the method used in W10, which is based on the halo occupation distribution (HOD) formalism. The HOD fully characterizes the number, velocity and spatial distribution of galaxies within dark matter halos. The probability distribution that a virialized dark matter halo of mass M will host N galaxies is designated as $P(N|M)$. $\langle N \rangle_M$ is the first moment of $P(N|M)$, and is the mean number of galaxies as a function of halo mass. Motivated by theory (e.g., Berlind et al. 2003; Kravtsov et al. 2004; Zheng et al. 2005), we consider central galaxies that live at the center of their host halo and satellite galaxies that orbit within the host potential as separate terms. We thus write the first moment of the HOD as $\langle N \rangle_M = 1 + \langle N_{\text{sat}} \rangle_M$. Furthermore, we assume that there is some minimum halo mass, M_{min} , below which a halo will contain no galaxies and above which there will always be at least one central galaxy. For the satellite component, we adopt the parametric form, $\langle N_{\text{sat}} \rangle_M = \exp[-M_0/(M_{\text{halo}} - M_{\text{min}})] \times (M_{\text{halo}}/M_1)^\alpha$, where the satellite galaxies obey a power-law function of slope α with an exponential cut-off at the low mass end at M_0 . M_1 is the characteristic mass scale where a halo will contain, on average, one central and one satellite galaxy.

To calculate the mean number of satellite galaxy pairs $\langle N_{\text{sat}}(N_{\text{sat}} - 1) \rangle$, the second moment of the satellite $P(N|M)$, we assume that the number of satellite galaxies in a halo of mass M follows a Poisson distribution of mean $\langle N_{\text{sat}} \rangle_M$. This sort of HOD parameterization is widely used to model galaxy clustering data (Zehavi et al. 2005a,b, 2011; Tinker et al. 2005; Conroy et al. 2006; Zheng et al. 2007, 2009; Watson et al. 2011).

Our fiducial model for characterizing the spatial distribution of galaxies within their host halos places one galaxy at the center and assuming that the satellites trace the underlying dark matter density distribution. The dark matter density profiles are described by the NFW relation $\rho(r) \propto (c \frac{r}{R_{\text{vir}}})^{-1} (1 + c \frac{r}{R_{\text{vir}}})^{-2}$ (Navarro et al. 1997), where c is the concentration parameter, $c \equiv R_{\text{vir}}/r_s$, and r_s is the characteristic scale radius. We use the virial definition of a halo to calculate the virial radius of host halos, such that $R_{\text{vir}} = ((3M)/(4\pi\Delta_{\text{vir}}\bar{\rho}))^{1/3}$, where Δ_{vir} is the mean halo overdensity ($\Delta_{\text{vir}} = 200$), and $\bar{\rho}$ is the mean density of the universe. The concentration - mass relation is given by Zheng et al. (2007) for the modification of Bullock et al. (2001): $c = \frac{c_0}{(1+z)} \times (\frac{M_{\text{halo}}}{M_*})^{-\beta}$, where $c_0 = 11$, M_* is the non-linear collapse mass at the median redshift of the sample for our choice of cosmology (M_* is redshift de-

TABLE 1
INPUT DATA FOR ALL LUMINOSITY SAMPLES

M_r	\bar{n}_g	z_{med}	$\log(M_*)$
-18.0	3.209 (0.169)	0.032	12.4228
-18.5	2.405 (0.131)	0.039	12.4147
-19.0	1.689 (0.092)	0.046	12.4057
-19.5	1.326 (0.058)	0.059	12.3887
-20.0	0.749 (0.018)	0.078	12.3647
-20.5	0.377 (0.009)	0.097	12.3397
-21.0	0.123 (0.002)	0.116	12.3057

NOTE. — \bar{n}_g is measured in units of $10^{-2} h^3 \text{Mpc}^{-3}$ and the associated error from 50 jackknife samples on the sky is shown in parentheses. z_{med} is the median redshift as measured in J11. M_* is the non-linear collapse mass and is in units of $h^{-1} M_\odot$.

pendent and is thus uniquely defined for each luminosity sample and is given in Table 1) and $\beta = 0.13$.

The mean number density of galaxies can be calculated for a given HOD by weighting the abundance of halos by $\langle N \rangle_M$ and integrating over all halo mass (see Eq.[2] of W10). We adopt the Warren et al. (2006) halo mass function, dn/dM , in all of our calculations, but our results are not sensitive to the specific choice of mass function.

To model the galaxy two-point correlation function (2PCF), ξ_{gg} , we use the halo model. ξ_{gg} can be decomposed into contributions due to galaxies residing in the same halo (the “one-halo” term) as well as galaxies living in separate, distinct halos (the “two-halo” term). Therefore, ξ_{gg} can be written as the sum of the one-halo and two-halo terms (e.g., Cooray & Sheth 2002; for this particular form of the equation see Zheng 2004): $\xi_{gg}(r) = \xi_{gg}^{1\text{halo}} + \xi_{gg}^{2\text{halo}} + 1$. Since we are probing such small scales we need only consider the one-halo term for modeling ξ . However, it is possible that omitting the two-halo term entirely could cause a bias in the best-fit parameters for the one-halo term. This bias would be largest for the dimmest galaxy sample, because these galaxies live in the smallest halos, and the two-halo term will become important at small scales. However, even for these galaxies the effect is limited. For instance, while it is true that isolated -18 galaxies will reside in halos with radii much smaller than $0.4h^{-1}\text{Mpc}$, the relevant halo size is set by M_1 . Furthermore, this is a threshold sample, so although the -18 sample will be dominated by galaxies of that brightness, there will still be much brighter galaxies that live in larger halos that influence M_1 . As seen in the upper-left panel of Fig. 3, $\langle M_1 \rangle$ for the -18 sample is $10^{12.77}$. This corresponds to a virial radius of order $0.4h^{-1}\text{Mpc}$. To carefully test the influence of the two-halo term, we have measured where the 1- and 2-halo terms cross for the -18 sample. This occurs at roughly $1h^{-1}\text{Mpc}$, so the influence of the 2-halo term at $0.4h^{-1}\text{Mpc}$ has a small effect on $w_p(r_p)$. We find that the amplitude of the 2-halo term is $\sim 7\%$ of the one-halo term at $0.4h^{-1}\text{Mpc}$ for the -18 sample. Nevertheless, we do approximately account for the effect of the 2-halo term on our modeling, and we discuss these assumptions in detail below.

The one-halo term depends on the second moment of $P(N|M)$, as well as the pair separation distributions of central-satellite and satellite-satellite pairs (see Eq.[4] of W10 for the particular form). The pair separation dis-

tribution for central-satellite pairs is essentially the same as the density profile of satellite galaxies. The satellite-satellite pair distribution is the convolution of the density profile with itself and, as in W10, we use the Sheth et al. (2001) calculation for the convolution of a truncated NFW profile with itself. Therefore, we can start to see the link between the shape of $\xi(r)$ and the shape of the satellite profile on small scales. This is discussed in detail in §4.

For each luminosity threshold, J11 measured the *projected* correlation function, so we convert our theoretical real-space correlation function $\xi(r)$ to $w_p(r_p)$ (Eq.[5] of W10). At each luminosity threshold, we integrate up to the π_{max} value given in Zehavi et al. (2011), which ranges from $40 - 60h^{-1}\text{Mpc}$. The method of J11 results in a π_{max} that is effectively larger than our choice. However, the difference is insignificant at the small scales we model. Integrating out to large scales means that the two-halo term cannot be entirely ignored. Since calculating the two-halo term correctly is fairly complex and its contribution to $w_p(r_p)$ is minimal at the scales of the data points that we model, we use a simple approximation instead. We use a two-halo term whose shape is the same as Zehavi et al. (2011), but whose amplitude can change with HOD parameters. Thus, for a given set of HOD parameters, we first calculate the large-scale bias of galaxies, b_g ,

$$b_g = \bar{n}_g^{-1} \int_{M_{\text{min}}}^{\infty} dM \frac{dn}{dM} b_h(M) \langle N \rangle_M, \quad (1)$$

where $b_h(M)$ is the large-scale bias of halos from Tinker et al. (2008). The two-halo term has a simple relation to the matter-matter correlation function on large scales: $\xi_{gg}^{2\text{halo}} = b_g^2 \xi_{mm}$. Thus, the relative two-halo terms of two different galaxy samples really only depends on the ratio of the bias of each sample. We consider the best-fit two-halo term from Zehavi et al. (2011) for each luminosity and append a newly defined two-halo term to our model one-halo term,

$$\xi_{gg}^{2\text{halo}} = \left(\frac{b_g}{b'_g} \right)^2 \xi_{gg}^{2\text{halo}'} , \quad (2)$$

where primes designate the Zehavi et al. (2011) values. In effect, we allow the amplitude of the 2-halo term to vary with HOD parameters, but we keep its shape fixed. The error introduced by this approximation is completely negligible as we have checked that even a shift as large as 20% in the amplitude of the two-halo term has no appreciable effect on $w_p(r_p)$ at the maximum pair separation that we consider ($0.4h^{-1}\text{Mpc}$) for any of the luminosity threshold samples. This test also emphasizes our insensitivity to the difference between our choice of integrating out to the π_{max} given by Zehavi et al. (2011) and the technique used by J11.

3.2. The PNM and PNMCG Models

W10 considered 4 distinct models for modeling the small-scale $w_p(r_p)$ of LRGs. In this paper we need only consider two of the models, defined as:

- **PNM** - in this model the only free parameters are those associated with the $P(N|M)$ distribution as described in §3.1 - M_{min} , M_0 , M_1 , and α . While

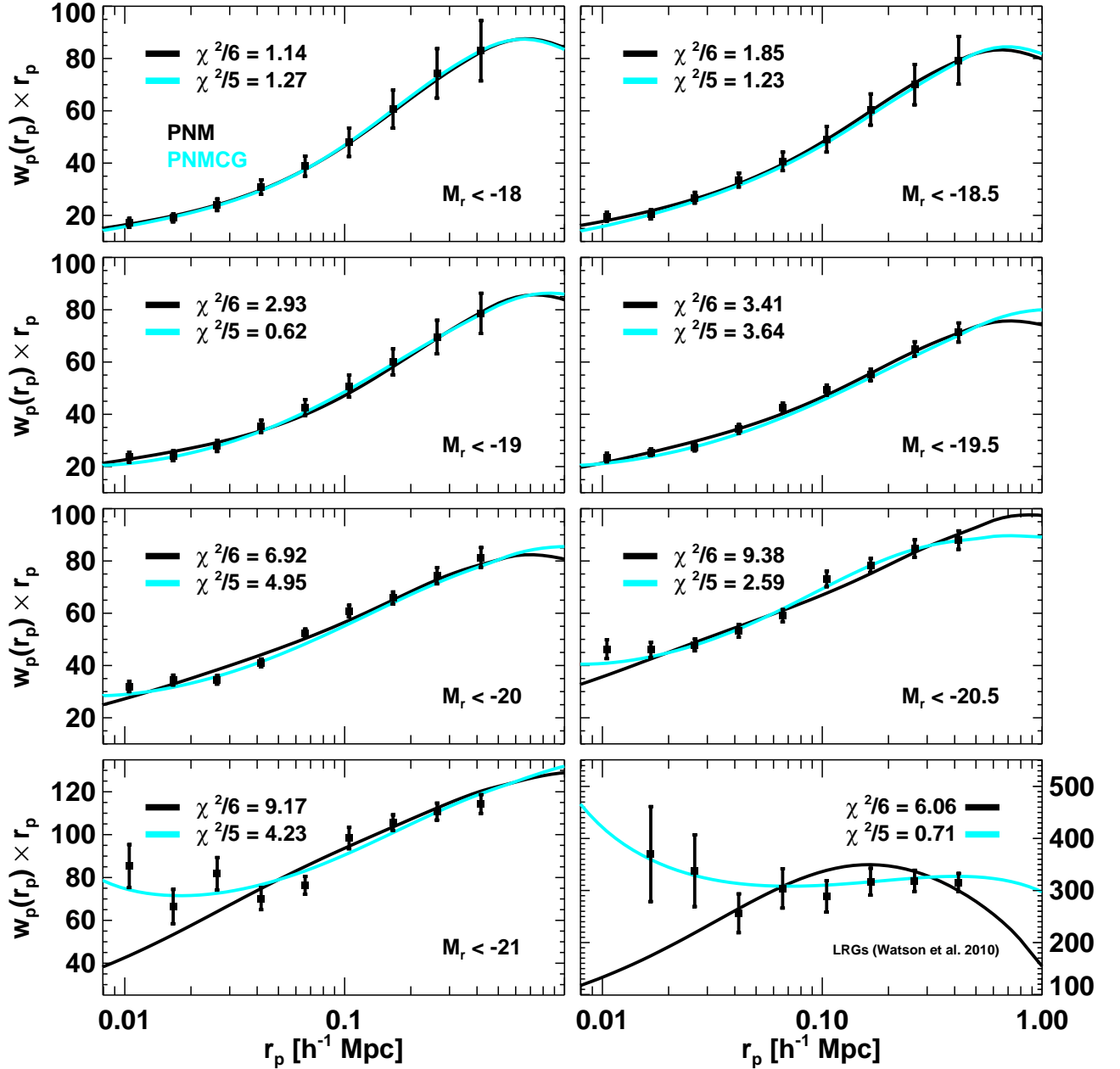


FIG. 1.— Model fits to the projected correlation function for luminosity thresholds spanning $M_r < -18$ to LRGs. The points in the $M_r < -18$ through $M_r < -21$ panels show the Jiang et al. (2011) $w_p(r_p)$ measurements (multiplied by r_p) and their associated jackknife errors. The bottom right panel shows results for LRGs from Watson et al. (2010). The black curves show the best-fit PNM models, which use four-free parameters describing the probability distribution $P(N|M)$ (M_{\min} , M_1 , M_0 , and α). The PNMCG model, shown in cyan, considers two additional free parameters (but M_0 is fixed to M_{\min}): (1) f_{gal} , which relates the concentration of the density profile of satellite galaxies relative to dark matter ($f_{\text{gal}} = c_{\text{gal}}/c$), and (2) γ , which allows for the inner slope of the density profile to differ from the dark matter distribution. The reduced χ^2 values for each best-fit model are listed in each panel.

these parameters are free to take on any value, the spatial distribution of satellite galaxies within halos is fixed to an NFW dark matter density profile. Since there are 10 data points (9 from the J11 $w_p(r_p)$ measurements along with the measured number density for each luminosity sample) and 4 free parameters, the PNM model has 6 degrees of freedom.

- **PNMCG** - this model allows for the same free parameters as the PNM model, with the exception of M_0 . M_0 was unconstrained in our initial MCMC runs (this was also the case in W10), thus we fixed M_0 to M_{\min} throughout our analysis. The PNMCG model also considers a parametrized density profile for satellite galaxies. As in W10, we allow both the concentration and the inner slope of the density profile to be free. The satellite galaxy concentra-

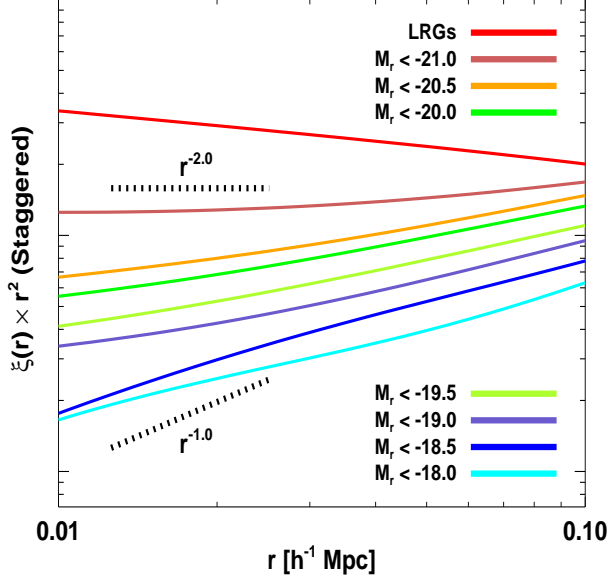


FIG. 2.— The real-space correlation function $\xi(r)$ residuals from an r^{-2} power law from the PNMCG best-fit models before converting to the projected correlation functions of Fig. 1. Amplitudes have been arbitrarily shifted for clarity. The slope of $\xi(r)$ on small scales is a reflection of the central-satellite pair distribution, which is essentially just the density profile itself. There is a strong luminosity dependence of the slope of $\xi(r)$ on small scales, becoming steeper and steeper for the brighter galaxy samples and this carries directly over to the luminosity dependence of the radial profile of satellite galaxies. The dotted lines show r^{-1} and r^{-2} power-law slopes.

tion can differ from the dark matter concentration (defined in §3.1) through the free parameter f_{gal} ,

$$c_{\text{gal}} = f_{\text{gal}} \times c. \quad (3)$$

The inner slope of the density profile is no longer fixed to -1, as is the case for an NFW profile, but rather is specified by the free parameter γ . As in W10, we adopt the following density profile for satellite galaxies

$$\rho(r) = \frac{\rho_s}{(c_{\text{gal}} \frac{r}{R_{\text{vir}}})^\gamma (1 + c_{\text{gal}} \frac{r}{R_{\text{vir}}})^{3-\gamma}}. \quad (4)$$

For an NFW profile $\gamma = 1$, however, the PNMCG model allows γ to take on any value from 0–4. This model considers the same number of data points as the PNM model, but now there are 5 free parameters (M_{min} , M_1 , α , f_{gal} and γ) resulting in 5 degrees of freedom.

As detailed in §3.4 of W10, we use a Markov Chain Monte Carlo (MCMC) method to probe the parameter space for a given set of parameters (see Dunkley et al. 2005 for details on MCMC techniques). When a chain has converged, we can find the most likely value for each parameter by calculating the mean of its distribution. Errors for each parameter are given by the extrema of the middle 68.3% of the distribution. Best-fit parameters are found by the combination of parameter values for which χ^2 is a minimum.

4. RESULTS

J11 measured $w_p(r_p)$ to very small scales over a large range in luminosity thresholds. Their measurements nicely overlap those of Zehavi et al. (2011) on intermediate scales ($\sim 0.2 - 7h^{-1}\text{Mpc}$, see Fig. 14 in J11), and extend down to very small scales with the innermost data point for each sample at $\sim 10h^{-1}\text{kpc}$. As discussed in §3.2, for each luminosity threshold sample, we model $w_p(r_p)$ with, (1) the PNM model, which only varies parameters that determine the number of galaxies in a given halo, but forces the satellite galaxies to have an NFW spatial distribution within their halo, and (2) the PNMCG model, which also allows the spatial distribution of satellite galaxies to vary within halos.

Figure 1 shows our modeling results for each luminosity sample. $w_p(r_p)$ has been scaled by an r_p^{-1} power law to more clearly highlight any discrepancies between the PNM and PNMCG models. Each panel shows the SDSS data points as well as the best-fit model for the PNM (black curve) and PNMCG (cyan curve) cases. It is clear from the figure that as we go to higher luminosities, the PNMCG model provides a significantly better fit to the data. We find that the $P(N|M)$ parameter distributions are nearly the same for the two models, differing by, at most, $\sim 3\sigma$. Therefore, the improved fits for the PNMCG model principally arise from the freedom to vary the density profile of satellite galaxies. Varying the density profile is thus necessary to find a better fit to the data as we go to higher luminosities.

We note that the reduced χ^2 values (listed in each panel) are in many cases quite high, even in the PNMCG case. This could mean that the PNMCG model contains incorrect assumptions or does not have enough freedom. On the other hand, it could mean that the J11 jackknife errors are underestimated. To check the impact of the error estimates on our modeling, we re-estimated errors for the $M_r < -20$ sample using mock galaxy catalogs from the LasDamas project (McBride et al. in prep.). We used 160 catalogs¹ and measured the dispersion of $w_p(r_p)$ between the catalogs, using the same binning method as J11. We then applied the fractional error (with respect to the mean of all mock measurements) to the data (non-mock) measurement to estimate the absolute errors and full covariance. Finally, using our new mock based error estimates, we re-ran the MCMC chains for the PNMCG model. We then compared the best-fit parameter values for the two fits and found that the parameters did not change significantly. By this, we mean the difference in χ^2 between the two best-fit points were within 1σ when evaluated with either of the likelihood surfaces (from each of the two MCMC runs with different errors). We conclude two things from this test: (1) our somewhat high χ^2 values are not overly concerning, and are likely due to a slight underestimate of the errors from jackknife re-sampling on the data, and (2) this issue does not seem to affect any of our conclusions.

We now investigate the luminosity dependence of the radial distribution of satellite galaxies and the degree to which it differs from an NFW distribution. As discussed in §3.1, when constructing the real-space correlation function in the halo model, the one-halo term considers contributions from central-satellite and satellite-

¹ North-only SDSS footprint from the LasDamas “gamma” data release.

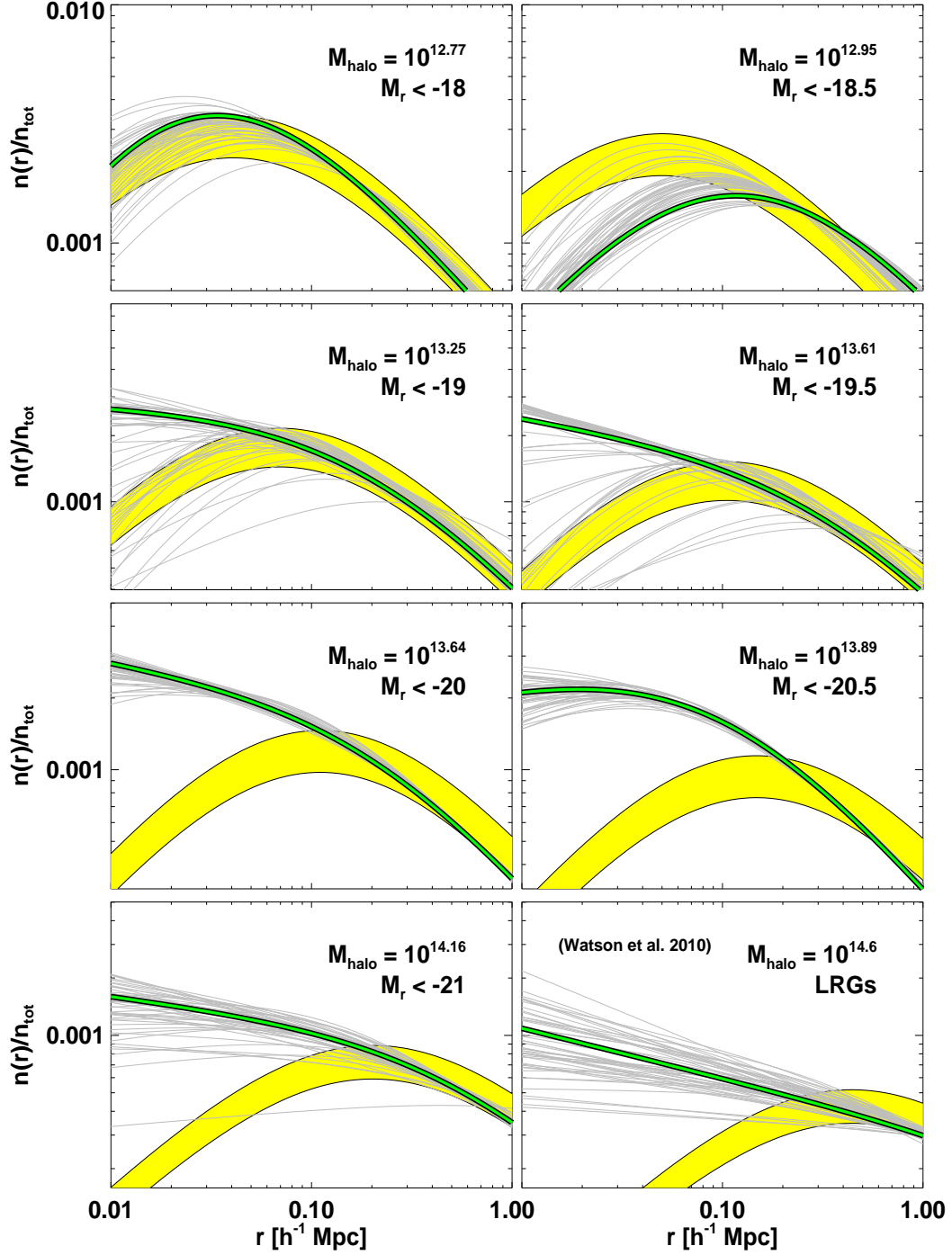


FIG. 3.— The radial profile of satellite galaxies as a function of luminosity. Each panel shows results for a specific luminosity sample, and for a halo mass that is chosen to be the mean value of M_1 from the PNMCG MCMC chain (listed in the top right of the panel). The solid, yellow bands show the NFW profile, with a 20% uncertainty to account for the possible ambiguity in the dark matter distribution. Green curves show the profile corresponding to the best-fit PNMCG model. Each panel also contains 50 grey curves representing 50 randomly drawn links from the top 95% of the PNMCG MCMC chain, after sorting in χ^2 from lowest to highest values. These 50 curves thus span the 95% confidence region allowed by the data. As we probe higher luminosities, the radial profile of satellite galaxies strongly deviates from an NFW distribution on small scales, showing that luminous galaxies are poor tracers of the underlying dark matter.

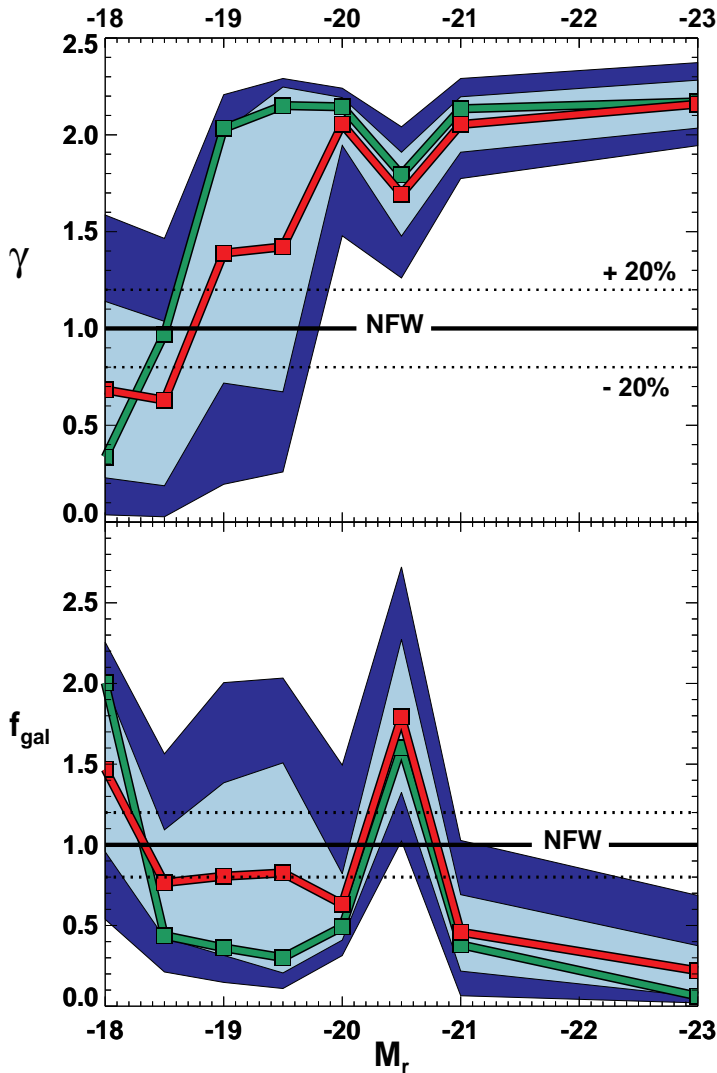


FIG. 4.— *Top Panel*: The slope of the inner density profile of satellite galaxies as a function of galaxy luminosity. The filled red squares (and connecting lines) show the mean value of γ from the MCMC chain of the PNMC model for each luminosity sample and the green squares represent the best fit. The light blue and dark blue bands are the associated errors from the extrema of the middle 68.3% and 95% of the distribution, respectively. $\gamma = 1$ corresponds to an inner slope for an NFW dark matter profile, and is shown as a solid black line. The dotted black lines highlight an assumed 20% inaccuracy in the dark matter profile. *Bottom Panel*: The same procedure as the top panel, but for the parameter f_{gal} which relates the galaxy and dark matter concentrations ($f_{\text{gal}} = c_{\text{gal}}/c$). f_{gal} and γ are intrinsically linked and there is a strong trend towards inner slopes becoming steeper than NFW as we go to higher luminosities, with corresponding decreasing values of f_{gal} .

satellite pairs. The central-satellite contribution, which is essentially just the density profile itself (see Eq. 4 of W10), is steeper than the satellite-satellite pair contribution and thus dominates the correlation function on the very small scales that we are considering (e.g., Figure 4. of Zheng et al. 2009). Therefore, the luminosity dependence of the *slope of $\xi(r)$ on small scales* can give a direct indication of the luminosity dependence of the *radial profile of satellite galaxies* (though the slope of $\xi(r)$ will be less steep than the slope of the radial density profile due to the dampening effect of the satellite-satellite

term). Figure 2 shows the residuals from an r^{-2} power law from the PNMC best-fit models before converting to the projected correlation functions shown in Figure 1. The amplitudes of the curves have been arbitrarily staggered simply to make the plot more clear. The dotted lines highlight the cases of r^{-1} and r^{-2} power laws. The slope of $\xi(r)$ is clearly a strong function of luminosity, being close to -1 for low luminosity galaxies and going more and more towards -2 for the $M_r < -21$ sample and even steeper for LRGs. The W10 result for the steepness of the slope of $\xi(r)$ for LRGs on small scales was also found by Almeida et al. (2008). Using the Bower et al. (2006) semi-analytic model applied to the Millenium simulation (Springel et al. 2005), they found that the LRG real-space correlation function follows an $\sim r^{-2.07}$ power law shape down to the $\sim 10h^{-1}\text{kpc}$ scale.

We next wish to directly investigate the radial profiles of satellite galaxies that are required by the data and compare them to the NFW profile. For each luminosity sample, we choose a halo mass equal to the mean value of M_1 in the PNMC MCMC chain for that sample. We choose M_1 because it represents the typical size halo that contributes central-satellite pairs to $\xi(r)$ (smaller halos have no satellites and larger halos are rare). Specifying the halo mass sets the amplitude, virial radius, and dark matter concentration in Equation 4. The radial profile then only depends on the parameters f_{gal} and γ . We then take the full MCMC chain for the PNMC model and sort it by χ^2 from lowest to highest. We then randomly draw 50 links from the top 95% of the chain. Each of these links has distinct values of f_{gal} and γ , which we insert into Equation 4 in order to construct individual radial profiles. The light grey curves in each panel of Figure 3 show these 50 profiles (multiplied by $4\pi r^2 dr$ to convert them from density into mass profiles). These curves thus span the 95% confidence region allowed by the data. The green curve in each panel shows the radial profile corresponding to the best-fit PNMC model. To compare with the NFW profile for dark matter, we also plot the case $f_{\text{gal}} = 1$, $\gamma = 1$, shown by the yellow bands. We assume that the dark matter profile of halos has a 20% uncertainty, which we represent as the thickness of the bands (see §5 for discussion of the uncertainties in the dark matter distribution in halos). For reference, the scale radius for any particular sample occurs where the dark matter radial profile “turns over”. Figure 3 shows, once again, that galaxies of increasing luminosity deviate more from an NFW profile. In fact, the figure seems to suggest that there is a transition point, somewhere between an absolute r -band magnitude of -19.5 and -20, where the radial profile of satellite galaxies goes from being consistent with NFW to completely inconsistent. For the highest luminosity samples, the profiles approach a power-law shape.

Figure 4 shows the luminosity dependence of the inner slope and concentration of satellite galaxies as found by the PNMC model. The dark blue and light blue bands in each panel represent the middle 95% and 68.3% of the MCMC chains after first sorting in γ (top panel) and sorting in f_{gal} (bottom panel). The filled red squares show the mean of the respective parameters in the MCMC chain for each luminosity sample and filled green squares show the best-fit values. The solid black line highlights the NFW dark matter inner slope of the

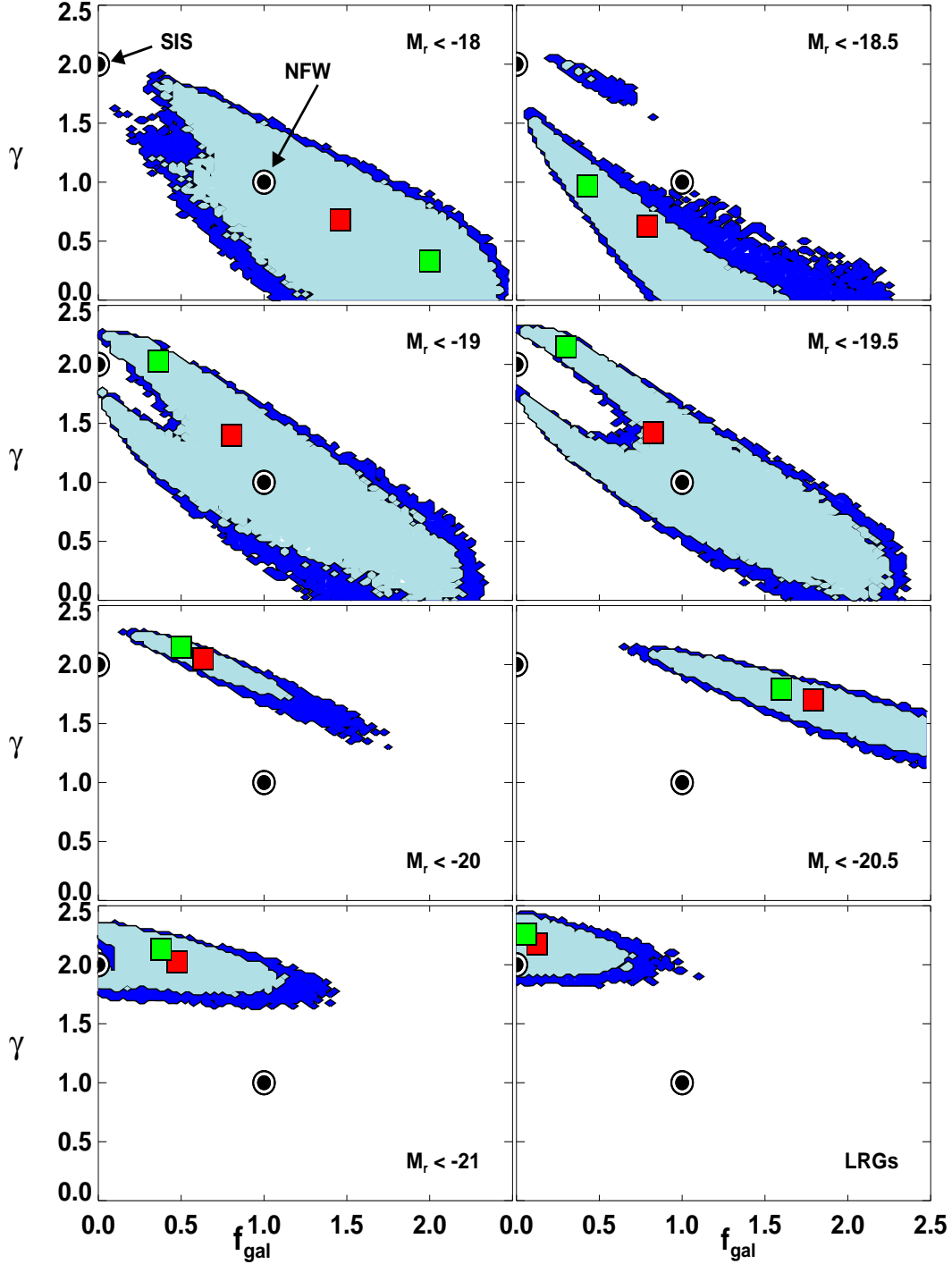


FIG. 5.— The γ – f_{gal} parameter space as a function of luminosity, highlighting the relationship between the inner slope and concentration of the density profile of satellite galaxies relative to dark matter. For each panel, the dark blue and light blue regions are defined as the top 95% and 68.3% of the MCMC chain for a given luminosity sample after sorting in χ^2 . There are two points of reference designated as filled circles - the $\gamma = 1, f_{\text{gal}} = 1$ combination that represents an NFW distribution, and the $\gamma = 2, f_{\text{gal}} \rightarrow 0$ combination that represents a singular isothermal sphere distribution (SIS). Red squares show the mean values of γ and f_{gal} from our MCMC runs and green squares show the values for the best-fit model. The data for $M_r < -20$ and brighter galaxies strongly rule out the NFW model and are in good agreement with an SIS distribution for $M_r < -21$ and LRGs.

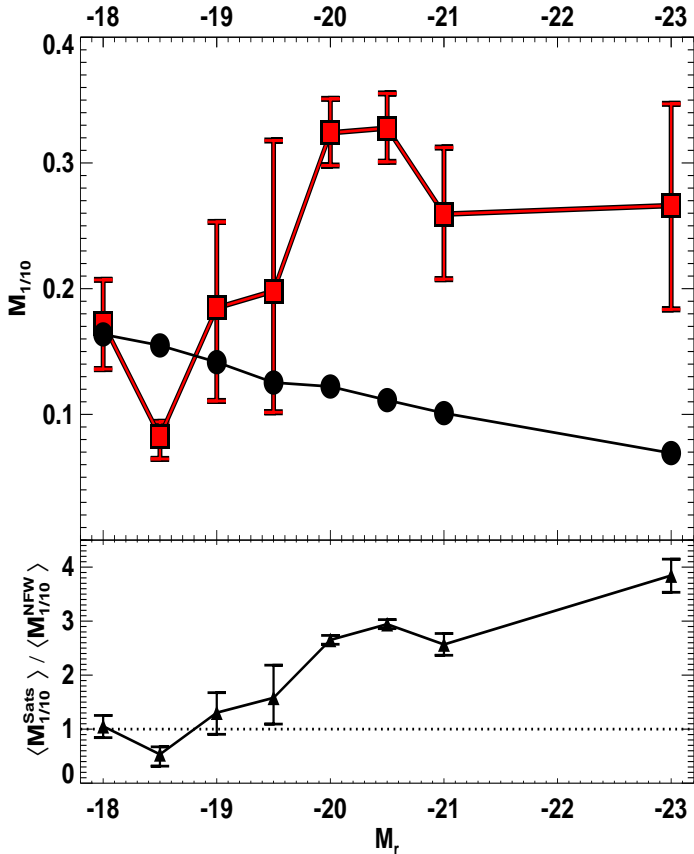


FIG. 6.— A more physically useful definition of concentration: $M_{1/10}$, defined as the fraction of satellite galaxies (or mass) that are enclosed within one tenth of the virial radius of a halo (see Eq. 5). *Top Panel:* For each luminosity sample, we choose a mass equal to the mean value of M_1 from the PNMCG MCMC chain, and we compute $M_{1/10}$ for each link in the chain. Red squares (and connecting lines) show the mean of the $M_{1/10}$ distribution for a given luminosity, and errorbars for $M_{1/10}$ show the extrema of the middle 68.3% of the distribution. Black points show $M_{1/10}$ for an NFW distribution. *Bottom Panel:* Ratio of $M_{1/10}$ for satellites with respect to dark matter. The dotted line highlights a ratio of unity. Satellite galaxies clearly become much more centrally concentrated than dark matter with increasing luminosity.

density profile which corresponds to $\gamma = f_{\text{gal}} = 1$ and the dotted lines represent the possible 20% ambiguity of an assumed NFW inner slope and concentration. The $M_r < -18, -18.5, -19$ and -19.5 samples have large spreads in γ and f_{gal} values, as there are many parameter combinations that can yield a similar goodness-of-fit to the data. For $M_r < -20$ and brighter galaxies, both γ and f_{gal} have tighter distributions and deviate from NFW. Figure 4 shows that there is a strong luminosity dependence of the satellite galaxy profile, i.e. γ is an increasing function of luminosity, and f_{gal} is a decreasing one. However, notice the unique coupling of f_{gal} and γ for the -20.5 case, where f_{gal} seems to deviate from the aforementioned trend. γ for -20.5 satellite galaxies also strays from the trend, but it is still significantly larger than NFW, and still lies within 1σ of the $M_r < -20$ and $M_r < -21$ values (f_{gal} is within 2σ). However, the reason for this outlier is unclear, though it may be due to the fact that $w_p(r_p)$ has a strong feature at roughly the

scale radius of the typical host halo (see the $M_r < -20.5$ panel of Fig. 1). This may cause a unique interplay between f_{gal} and γ , resulting in a mild departure from the trends. For $M_r < -20$ and brighter galaxies, the mean value of γ ranges between 1.6 - 2.1, significantly steeper than NFW. This range of γ values persists all the way down to $M_r < -19$ when considering the best-fit values. As mentioned in §2, M06 found a systematic error in the manner that light in the overlapping region of LRG pairs was being allocated in the SDSS pipeline. This caused a slight boost in the small-scale correlation function and was corrected for by M06. This effect is expected to rapidly diminish for lower luminosity samples, because the intrinsic sizes of galaxies will be smaller. However, we apply the same LRG correction to the J11 $M_r < -21$ sample to model the maximum effect that this could have. While we expect $\langle \gamma \rangle$ to decrease as a result of the innermost data points being scaled to lower $w_p(r_p)$ values, we still find that $\langle \gamma \rangle \sim 1.6$. Thus, even after assuming a *drastic* over-correction, γ is still strongly discrepant from NFW.

Figure 4 showed the luminosity trends for γ and f_{gal} by sorting the MCMC chains separately for each parameter. However, γ and f_{gal} are intrinsically coupled to one another so it is important to investigate the joint $\gamma - f_{\text{gal}}$ parameter space. Figure 5 Shows the $\gamma - f_{\text{gal}}$ parameter space at each luminosity, with the dark blue and light blue regions defined as the top 95% and 68.3% of the MCMC chain, after sorting in χ^2 . There are two points of reference designated as filled circles: the $\gamma = 1, f_{\text{gal}} = 1$ combination for an NFW distribution and a $\gamma = 2, f_{\text{gal}} \rightarrow 0$ combination representing a singular isothermal sphere (SIS) distribution. Red squares represent the mean values of γ and f_{gal} from our MCMC runs and green squares show the best-fit combination. As expected, the $M_r < -18$ through -19.5 exhibit a broad range in $\gamma - f_{\text{gal}}$ combinations, with the NFW combination lying within the top 68.3% region (with the exception of the -18.5 sample). The $\gamma - f_{\text{gal}}$ regions clearly drift away from NFW for $M_r < -20$ and greater luminosities and are well described by an SIS distribution for both the -21 and LRG samples. Figure 5 shows that the inner slope and concentration parameters are strongly degenerate with each other, particularly at low luminosities. This can be caused by having the scale radius (the radius within the halo where the slope transitions from $-\gamma$ to -3) too close to the innermost data point. When this happens, the data cannot accurately constrain the inner slope, and only constrains γ and f_{gal} through their degenerate contribution to the amplitude of the density profile. A simple calculation of the scale radius using the virial definition of a halo (see §3.1) gives $r_s \sim 10h^{-1}\text{kpc}$ for the $M_r < -18$ sample (adopting a halo mass equal to the mean value of M_1), which is precisely at the scale of the innermost data point of $w_p(r_p)$. This leads to the large spread in $\gamma - f_{\text{gal}}$ combinations. Of course, as we go to brighter samples, the scale radii increase, and the parameters are better constrained.

For each luminosity, as the inner profile steepens, f_{gal} decreases (with the slight deviation for the $M_r < -20.5$ case). The decrease in concentration does not necessarily imply that the concentration of satellites is low in the traditional sense - i.e., that there are fewer galaxies at small radii - but rather that the radial profiles simply

evolve toward a more power-law form. For example, as $f_{\text{gal}} \rightarrow 0$ in the case of LRGs, this does not mean that the LRG satellites are less concentrated than the underlying dark matter. As $f_{\text{gal}} \rightarrow 0$, the scale radius is pushed far outside the virial radius, resulting in a pure power-law distribution of slope $-\gamma$. Since the value of f_{gal} can be misleading when thinking about the concentration of satellite galaxies, we consider an alternative definition of “concentration” that is more physically useful: the fraction of satellite galaxies (or mass) that are enclosed within a tenth of the virial radius R_{vir} . We call this quantity $M_{1/10}$ and compute it by integrating any radial profile out to one-tenth the virial radius of the host halo and dividing by the total mass out to R_{vir}

$$M_{1/10} = \frac{M(r < 0.1R_{\text{vir}})}{M(r < R_{\text{vir}})}. \quad (5)$$

Figure 6 (top panel) shows $M_{1/10}$ as a function of luminosity. For each luminosity sample, we assume a halo mass equal to the mean value of M_1 from the MCMC chain, and we calculate $M_{1/10}$ for every link in the chain using each link’s values for γ and f_{gal} . We then find the mean of the distribution of $M_{1/10}$ values (denoted by the red squares and connecting lines). Errors for $M_{1/10}$ are given by the extrema of the middle 68.3% of the distribution after sorting by $M_{1/10}$. The black filled circles show $M_{1/10}$ for a dark matter NFW profile. The dark matter concentration drops with luminosity because the mean value of M_1 increases with luminosity and concentration is a decreasing function of halo mass (Bullock et al. 2001). The bottom panel of Figure 6 shows the ratio of $M_{1/10}$ for satellites with respect to dark matter. The figure clearly shows that low luminosity satellite galaxies ($M_r > -19.5$) have spatial concentrations similar to dark matter, whereas the profiles of luminous satellite galaxies ($M_r < -20$ and brighter) are $\sim 2.5 - 4$ times more concentrated than NFW.

5. SUMMARY & DISCUSSION

Do satellite galaxies trace the underlying dark matter distribution? Our modeling of the small-scale $w_p(r_p)$ over an enormous range in galaxy luminosity thresholds, from SDSS Main galaxies to LRGs ($M_r < -18$ through $\lesssim -23$), has revealed a strong luminosity dependence of the radial distribution of satellite galaxies. We have found that for the low luminosity samples (lower than $M_r < -20$), there is a wide range of satellite galaxy concentrations (equal to f_{gal} times the NFW dark matter concentration) and inner density profile slopes, $-\gamma$, that are consistent with the data. This lack of constraining power is due to a strong degeneracy between f_{gal} and γ , which, in turn, is possibly due to the fact that the smallest scale data point in $w_p(r_p)$ is roughly around the scale radius for halos hosting galaxies of this size. Nevertheless, low luminosity satellite galaxies have radial distributions that are generally consistent with the NFW dark matter distribution. When we move to higher luminosity galaxies ($M_r < -20$ and brighter samples) however, satellite profiles change dramatically, with the most striking feature being that γ jumps to much higher values. Our results show that for $M_r < -20$ and brighter galaxies, γ ranges from $\sim 1.6 - 2.1$, highly discrepant from NFW, even after assuming a 20% inaccuracy in the dark matter profile. Luminous satellite galaxies are thus poor

tracers of the underlying dark matter within halos on the small scales that we probe. Since the effects of f_{gal} and γ on the radial profile are intertwined, we have calculated a more physically useful quantity $M_{1/10}$, which gives the fractional amount of mass enclosed within one-tenth of the virial radius. We find that $M_{1/10}$ is a strong function of luminosity, being consistent with NFW for low luminosity galaxies and being $\sim 2.5 - 4$ times more concentrated than NFW for galaxies brighter than $M_r < -20$.

Several other studies have also investigated the radial distribution of galaxies within halos. When considering faint satellites around $\sim L^*$ galaxies, no consensus emerges. Chen (2009) found the satellite distribution to be consistent with NFW. More et al. (2009) found a cored satellite profile best described by a $\gamma = 0, f_{\text{gal}} = 0.5$ combination, inconsistent with NFW. Carlberg et al. (2009) found that the radial profiles of dwarf satellites around nearby galaxies are much *more* concentrated than NFW, rendering all of these studies in disaccord. Furthermore, the discrepancies persist when considering a broader range of galaxy systems. Nierenberg et al. (2011) recently studied the radial profile of satellites around massive, early-type galaxies at intermediate redshifts. Assuming a power-law profile model, they find that the satellites have an isothermal distribution of slope -1 . Guo et al. (2012) considered SDSS satellite galaxies around host central galaxies of a wide luminosity range and, in general, satellite number density profiles were shown to be consistent with NFW. The NFW dark matter concentration was found to decrease with increasing satellite galaxy luminosity, independent of the host galaxy luminosity (except for the brightest centrals). They also detected a slightly *steeper* profile for *fainter* satellites. These varying results imply that uncovering the spatial distribution of satellite galaxies is a difficult problem. In the end, we have found that there is a strong luminosity dependence of the radial distribution of satellite galaxies, wherein $\sim L^*$ and brighter satellites within group and cluster sized halos have a *substantially steeper* radial profile than dark matter on scales smaller than $\sim 100h^{-1}\text{kpc}$. We emphasize that while the scales involved in all of these studies are similar to ours, galaxy sample selection is different in each case, making it difficult to directly compare their results with ours.

Our results have shown that luminous galaxies are poor tracers of NFW. We now address the possibility that NFW is a poor model for the underlying dark matter distribution. In the established ΛCDM concordance cosmology, recent studies invoking high resolution N-body simulations have shown that the mass profiles of ΛCDM halos slightly, but systematically, deviate from NFW, becoming shallower at smaller radii (Stadel et al. 2009; Del Popolo 2010). In fact, they may be better described by Einasto profiles, which include a parameter α that controls how the logarithmic slope will vary with radius to accurately account for the fact that halo profiles seem to not be self-similar (Gao et al. 2008; Navarro et al. 2010; Ludlow et al. 2010). These studies find, on average, $\gamma < 1$ (Graham et al. 2006; Navarro et al. 2010). However, on average, the simpler, two-parameter NFW model, which has a characteristic r^{-1} inner slope, is accurate to within 10 – 20% (Benson 2010). Moreover, Mandelbaum et al. (2008) fit galaxy cluster weak lensing profiles on small scales and found that NFW and

Einasto profiles gave the same result to within several percent. Therefore, for simplicity, and to be consistent with previous modeling of LRGs by Watson et al. (2010), we assumed an NFW distribution throughout our modeling analysis. We conclude from the aforementioned studies that NFW is not a poor model for the dark matter distribution in collisionless simulations and, to the extent that it is, the true profile is even more discrepant from our results for luminous satellite galaxies.

Of course, by assuming a pure dark matter profile established from high resolution N-body simulations, the effects that baryons can have on dark matter are not considered. *Adiabatic Contraction* (AC) (Blumenthal et al. 1986; Ryden & Gunn 1987; Gnedin et al. 2004) may cause a steepening of the inner slope of the dark matter density profile as the gas condenses and sinks to the center of the dark matter potential well (Diemand et al. 2004; Fukushige et al. 2004; Reed et al. 2005; Del Popolo & Kroupa 2009). However, the majority of results indicate that the steepening is insubstantial or can vary widely from halo to halo (e.g., Tissera et al. 2010). In fact, while AC may cause a steepening of the inner profile, over time, major and minor mergers can cause the dark matter profile to become shallower. (El-Zant et al. 2001; Romano-Díaz et al. 2008, 2009; Johansson et al. 2009). Observational confirmations of AC are notoriously difficult. In the case of galaxy clusters, X-ray analysis by Zappacosta et al. (2006) showed that processes during halo formation (e.g. gravitational heating from merger events) counteract AC and the mass profiles were still well described by NFW. Mandelbaum et al. (2006) used galaxy-galaxy lensing to show that the mass density profile of LRG clusters is consistent with NFW. Recently, Schulz et al. (2010) studied the profiles of a large sample of SDSS ellipticals and found that their dynamical mass measurements suggest that the measured excess mass on small scales *may* be consistent with the AC hypothesis. However, for bright galaxies, our results are still not reconcilable with current AC models. We thus conclude that luminous satellite galaxies are indeed poor tracers of the underlying dark

matter distribution, even accounting for the effects of baryons on the dark matter.

It is perhaps not surprising that galaxies do not behave like test particles as they orbit within a dark matter potential well. Being massive and extended, they are subject to dynamical mechanisms that would not affect test particles, namely dynamical friction and mass loss due to the tidal field of their host halo. In fact, these mechanisms should affect large and massive objects more than small ones, which could explain the luminosity trend that we observe. Satellite galaxies are thought to reside within subhalos, so it makes more sense to compare the radial distribution of galaxies to that of subhalos, rather than just dark matter. While subhalos tend to have a less concentrated radial distribution than dark matter (Ghigna et al. 1998, 2000; Gao et al. 2004; De Lucia et al. 2004; Nagai & Kravtsov 2005), the subhalo distribution has yet to be extended down to the extreme small scales that we have probed. High resolution N-body simulations are just now becoming available that allow for subhalos to be distinguished at the $10h^{-1}\text{kpc}$ separation level (e.g., Klypin et al. 2010) for all of the luminosity samples that we have studied. Of course, subhalos may not be perfect tracers of galaxies, but it will be interesting to see whether the distribution of subhalos as a function of mass follows the same trend that we have uncovered for satellite galaxies as a function of luminosity. If the primary cause of this trend is dynamical in nature (e.g., dynamical friction), it should also show up with subhalos. Either way, such a comparison will yield insight into the relation between subhalos and galaxies on very small scales, as well as the complicated non-linear processes occurring towards the centers of host halos, crucial for galaxy formation theory.

6. ACKNOWLEDGEMENTS

AAB is supported by Vanderbilt University and the Alfred P. Sloan Foundation. We thank Zheng Zheng for providing us with his best-fit 2-halo term for all the galaxy samples.

REFERENCES

- Abazajian, K. N., et al. 2009, *ApJS*, 182, 543
 Almeida, C., Baugh, C. M., Wake, D. A., Lacey, C. G., Benson, A. J., Bower, R. G., & Pimbblet, K. 2008, *MNRAS*, 386, 2145
 Benson, A. J. 2010, *Phys. Rep.*, 495, 33
 Berlind, A. A., & Weinberg, D. H. 2002, *ApJ*, 575, 587
 Berlind, A. A., et al. 2003, *ApJ*, 593, 1
 Blanton, M. R., et al. 2003, *ApJ*, 594, 186
 ——. 2005, *AJ*, 129, 2562
 Blumenthal, G. R., Faber, S. M., Flores, R., & Primack, J. R. 1986, *ApJ*, 301, 27
 Bower, R. G., Benson, A. J., Malbon, R., Helly, J. C., Frenk, C. S., Baugh, C. M., Cole, S., & Lacey, C. G. 2006, *MNRAS*, 370, 645
 Bullock, J. S., Kolatt, T. S., Sigad, Y., Somerville, R. S., Kravtsov, A. V., Klypin, A. A., Primack, J. R., & Dekel, A. 2001, *MNRAS*, 321, 559
 Carlberg, R. G., Sullivan, M., & Le Borgne, D. 2009, *ApJ*, 694, 1131
 Chen, J. 2009, *A&A*, 494, 867
 Conroy, C., Wechsler, R. H., & Kravtsov, A. V. 2006, *ApJ*, 647, 201
 Cooray, A., & Sheth, R. 2002, *Phys. Rep.*, 372, 1
 De Lucia, G., Kauffmann, G., Springel, V., White, S. D. M., Lanzoni, B., Stoehr, F., Tormen, G., & Yoshida, N. 2004, *MNRAS*, 348, 333
 Del Popolo, A. 2010, *MNRAS*, 408, 1808
 Del Popolo, A., & Kroupa, P. 2009, *ArXiv e-prints*
 Diemand, J., Moore, B., & Stadel, J. 2004, *MNRAS*, 353, 624
 Dunkley, J., Bucher, M., Ferreira, P. G., Moodley, K., & Skordis, C. 2005, *MNRAS*, 356, 925
 El-Zant, A., Shlosman, I., & Hoffman, Y. 2001, *ApJ*, 560, 636
 Fukushige, T., Kawai, A., & Makino, J. 2004, *ApJ*, 606, 625
 Gao, L., De Lucia, G., White, S. D. M., & Jenkins, A. 2004, *MNRAS*, 352, L1
 Gao, L., Navarro, J. F., Cole, S., Frenk, C. S., White, S. D. M., Springel, V., Jenkins, A., & Neto, A. F. 2008, *MNRAS*, 387, 536
 Ghigna, S., Moore, B., Governato, F., Lake, G., Quinn, T., & Stadel, J. 1998, *MNRAS*, 300, 146
 ——. 2000, *ApJ*, 544, 616
 Gnedin, O. Y., Kravtsov, A. V., Klypin, A. A., & Nagai, D. 2004, *ApJ*, 616, 16
 Graham, A. W., Merritt, D., Moore, B., Diemand, J., & Terzić, B. 2006, *AJ*, 132, 2701
 Guo, Q., Cole, S., Eke, V., & Frenk, C. 2012, *ArXiv e-prints*
 Jiang, T., Hogg, D. W., & Blanton, M. R. 2011, *ArXiv e-prints*
 Johansson, P. H., Naab, T., & Ostriker, J. P. 2009, *ApJ*, 697, L38
 Klypin, A., Trujillo-Gomez, S., & Primack, J. 2010, *ArXiv e-prints*
 Kravtsov, A. V., Berlind, A. A., Wechsler, R. H., Klypin, A. A., Gottlöber, S., Allgood, B., & Primack, J. R. 2004, *ApJ*, 609, 35

- Ludlow, A. D., Navarro, J. F., Springel, V., Vogelsberger, M., Wang, J., White, S. D. M., Jenkins, A., & Frenk, C. S. 2010, *MNRAS*, 406, 137
- Mandelbaum, R., Seljak, U., Cool, R. J., Blanton, M., Hirata, C. M., & Brinkmann, J. 2006, *MNRAS*, 372, 758
- Mandelbaum, R., Seljak, U., & Hirata, C. M. 2008, *J. Cosmology Astroparticle Phys.*, 8, 6
- Masjedi, M., Hogg, D. W., & Blanton, M. R. 2008, *ApJ*, 679, 260
- Masjedi, M., et al. 2006, *ApJ*, 644, 54
- More, S., van den Bosch, F. C., Cacciato, M., Mo, H. J., Yang, X., & Li, R. 2009, *MNRAS*, 392, 801
- Nagai, D., & Kravtsov, A. V. 2005, *ApJ*, 618, 557
- Navarro, J. F., Frenk, C. S., & White, S. D. M. 1997, *ApJ*, 490, 493
- Navarro, J. F., et al. 2010, *MNRAS*, 402, 21
- Nierenberg, A. M., Auger, M. W., Treu, T., Marshall, P. J., & Fassnacht, C. D. 2011, *ApJ*, 731, 44
- Peacock, J. A., & Smith, R. E. 2000, *MNRAS*, 318, 1144
- Reed, D., Governato, F., Verde, L., Gardner, J., Quinn, T., Stadel, J., Merritt, D., & Lake, G. 2005, *MNRAS*, 357, 82
- Romano-Díaz, E., Shlosman, I., Heller, C., & Hoffman, Y. 2009, *ApJ*, 702, 1250
- Romano-Díaz, E., Shlosman, I., Hoffman, Y., & Heller, C. 2008, *ApJ*, 685, L105
- Ryden, B. S., & Gunn, J. E. 1987, *ApJ*, 318, 15
- Schulz, A. E., Mandelbaum, R., & Padmanabhan, N. 2010, *MNRAS*, 408, 1463
- Scoccimarro, R., Sheth, R. K., Hui, L., & Jain, B. 2001, *ApJ*, 546, 20
- Sheth, R. K., Diaferio, A., Hui, L., & Scoccimarro, R. 2001, *MNRAS*, 326, 463
- Springel, V., et al. 2005, *Nature*, 435, 629
- Stadel, J., Potter, D., Moore, B., Diemand, J., Madau, P., Zemp, M., Kuhlen, M., & Quilis, V. 2009, *MNRAS*, 398, L21
- Strauss, M. A., et al. 2002, *AJ*, 124, 1810
- Tinker, J., Kravtsov, A. V., Klypin, A., Abazajian, K., Warren, M., Yepes, G., Gottlöber, S., & Holz, D. E. 2008, *ApJ*, 688, 709
- Tinker, J. L., Weinberg, D. H., Zheng, Z., & Zehavi, I. 2005, *ApJ*, 631, 41
- Tissera, P. B., White, S. D. M., Pedrosa, S., & Scannapieco, C. 2010, *MNRAS*, 406, 922
- Warren, M. S., Abazajian, K., Holz, D. E., & Teodoro, L. 2006, *ApJ*, 646, 881
- Watson, D. F., Berlind, A. A., McBride, C. K., & Masjedi, M. 2010, *ApJ*, 709, 115
- Watson, D. F., Berlind, A. A., & Zentner, A. R. 2011, *ApJ*, 738, 22
- York, D. G., et al. 2000, *AJ*, 120, 1579
- Zappacosta, L., Buote, D. A., Gastaldello, F., Humphrey, P. J., Bullock, J., Brighenti, F., & Mathews, W. 2006, *ApJ*, 650, 777
- Zehavi, I., et al. 2005a, *ApJ*, 621, 22
- . 2004, *ApJ*, 608, 16
- . 2011, *ApJ*, 736, 59
- . 2005b, *ApJ*, 630, 1
- Zheng, Z. 2004, *ApJ*, 610, 61
- Zheng, Z., et al. 2005, *ApJ*, 633, 791
- Zheng, Z., Coil, A. L., & Zehavi, I. 2007, *ApJ*, 667, 760
- Zheng, Z., Zehavi, I., Eisenstein, D. J., Weinberg, D. H., & Jing, Y. P. 2009, *ApJ*, 707, 554